



**HAL**  
open science

## Bayesian uncertainty analysis of inversion models applied to the inference of thermal properties of walls

Séverine Demeyer, V. Le Sant, A. Koenen, N. Fischer, Julien Waeytens, Rémi  
Bouchié

► **To cite this version:**

Séverine Demeyer, V. Le Sant, A. Koenen, N. Fischer, Julien Waeytens, et al.. Bayesian uncertainty analysis of inversion models applied to the inference of thermal properties of walls. *Energy and Buildings*, 2021, 249, pp.111188. 10.1016/j.enbuild.2021.111188 . hal-04353797

**HAL Id: hal-04353797**

**<https://hal.science/hal-04353797>**

Submitted on 19 Dec 2023

**HAL** is a multi-disciplinary open access archive for the deposit and dissemination of scientific research documents, whether they are published or not. The documents may come from teaching and research institutions in France or abroad, or from public or private research centers.

L'archive ouverte pluridisciplinaire **HAL**, est destinée au dépôt et à la diffusion de documents scientifiques de niveau recherche, publiés ou non, émanant des établissements d'enseignement et de recherche français ou étrangers, des laboratoires publics ou privés.

1 **Bayesian uncertainty analysis of inversion models**  
2 **applied to the inference of thermal properties of**  
3 **walls**

4 **S everine Demeyer\*, V. Le Sant, A. Koenen and N. Fischer**

5 Laboratoire National de M etrologie et d'Essais, 29 avenue Roger Hennequin, 78197  
6 Trappes Cedex

7 \*E-mail: severine.demeyer@lne.fr

8 **Julien Waeytens**

9 Univ. Gustave Eiffel, IFSTTAR,  
10 14-20 boulevard Newton, 77447, Marne la Vall ee Cedex 2, France  
11 E-mail: julien.waeytens@univ-eiffel.fr

12 **R emi Bouchi e**

13 Centre Scientifique et Technique du B atiment,  
14 84 avenue Jean Jaur es, Champs-sur-Marne, 77447 Marne-la-Vall ee, France  
15 E-mail: remi.bouchie@cstb.fr

16 **Abstract.**

17 In this work, we propose a fully Bayesian uncertainty analysis of the indirect  
18 measurement of thermal properties of walls from in-situ temperature and flux  
19 measurements, obtained with an active method, using a one dimensional transient  
20 thermal model. We show that this approach is able to take into account the uncertainty  
21 of the inputs of the thermal model and the uncertainty of the output observations, for  
22 a more reliable uncertainty estimation of the *calibration parameters* and any derived  
23 quantity. For this problem, we improve the classical Bayesian inversion model by taking  
24 into account underestimated uncertainty on reported output observations, which is a  
25 frequently encountered issue in practice. We provide some recommendations for a wider  
26 applicability of the method. We illustrate the principles of uncertainty evaluation of the  
27 *Guide to the Expression of Uncertainty in Measurement* [BIPM et al., 2008a] in terms  
28 of a real case study to evaluate the thermal resistance of a multilayer wall placed in a  
29 climatic chamber. For this application, we compare results of the Bayesian inversion  
30 with classical steady-state results in comparable experimental conditions. We perform  
31 a sensitivity analysis to study the effect of duration and input uncertainties and we  
32 make recommendations. R code is made available that enables a Bayesian uncertainty  
33 evaluation of inversion models for related applications.

## 34 1. Introduction

35 In the context of building energy management or retrofit interventions, thermal  
 36 resistance of walls is used in standard heat transfer models as a parameter for  
 37 building performance simulations [Iglesias et al., 2018]. Due to the cost of wall thermal  
 38 characterization, tabulated values for thermal properties are typically used as inputs of  
 39 the energy models [Iglesias et al., 2018].

40 The in-situ measurement of the thermal resistance of walls should, for instance,  
 41 contribute to decrease the gap between actual and predicted consumption to have  
 42 more reliable energy-savings strategies or to have a more reliable assessment of the  
 43 effectiveness of retrofit interventions [Simon et al., 2018].

44 The present study is part of the French National Research project named RESBATI  
 45 whose main objective is to develop a portable measurement device for evaluating the  
 46 thermal resistance of opaque building walls on site. The result of the thermal resistance  
 47 measurement should be provided with its uncertainty [Ha et al., 2020]. The active  
 48 method (a thermal gradient inside the wall is created by a step heating excitation applied  
 49 on a face) chosen in the project allows to estimate the thermal resistance of a building  
 50 wall in all seasons, for any type of building and use (occupied or otherwise) in quite a  
 51 short measurement time (less than three days) which improves on classical steady-state  
 52 or dynamic methods [François et al., 2020], [Ha et al., 2020]. In this paper, we consider  
 53 that the thermal resistance of a wall is measured indirectly from in-situ temperature  
 54 and flux measurements. This is an inverse problem classically encountered in building  
 55 physics [Rouchier, 2018].

56 To carry out the identification method, a direct model (here a thermal model)  
 57 is embedded in a simulator  $\eta(X, \theta)$  whose inputs are the calibration parameters  $\theta$   
 58 (called *primary unknowns* in [Kaipio and Fox, 2011]), and the experimental conditions  
 59  $X$ , see Figure 1. In practice, [Kaipio and Fox, 2011] mention that it is very seldom that  
 60 the primary unknowns  $\theta$  are the only *input unknowns*. The vector  $X$  gathers all the  
 61 uncertainty sources, called here *input parameters*, having an effect on the measurement  
 62 result of the thermal resistance and that can be modeled by a probability distribution.  
 63 In the following, the uppercase notation  $X$  denotes a random vector, whereas the  
 64 lowercase  $x$  denotes a particular observed value of  $X$ . In this paper, we have chosen  
 65 a one-dimensional transient thermal model as a good approximation of the physical  
 66 phenomenon with a low computational cost. Since the thermal model does not take  
 67 into account lateral flux in the building wall, the user has to make sure that the flux is  
 68 close to 1D, which makes the simulator fit for purpose.

69 The identification process, illustrated in Figure 1, also called calibration or  
 70 inversion, consists to find the values  $\hat{\theta}$  of the input calibration parameters of the  
 71 thermal model so that the output  $\eta(x, \hat{\theta})$  is as closed as possible to the experimental  
 72 values  $y(x)$  obtained in the experimental conditions  $x$ . The classical techniques  
 73 for solving the minimization problem pertaining to inversion are based on least  
 74 squares methods (e.g. Levenberg-Marquardt algorithm), maximum-likelihood (ML) and

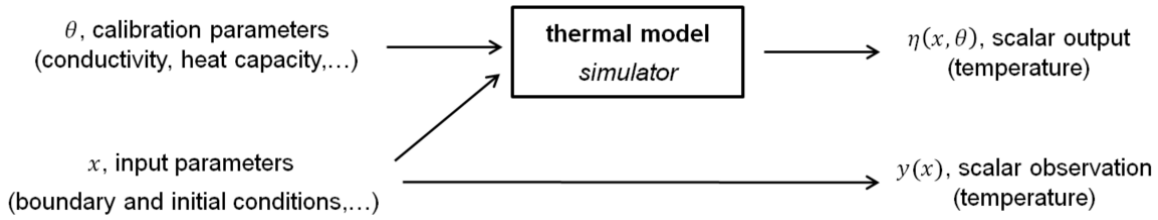


**Figure 1.** Schema of a calibration (inversion) procedure.

75 Bayesian analysis. A description and a comparison of these inversion techniques can  
 76 be found in [Rouchier, 2018] and [Kaipio and Fox, 2011]. In Bayesian statistics, the  
 77 inverse problem is regularized statistically through the modeling of prior distribution  
 78 [Kaipio and Fox, 2011]. Prior distributions represent prior degrees of belief on the  
 79 (usually) unique but unknown values of the inputs which are turned into posterior  
 80 degrees of belief (posterior distributions) via the Bayes formula when observations are  
 81 available. The reader interested in generalities about Bayesian statistics can refer to  
 82 [Gelman et al., 2013] and [Box and Tiao, 1992].

83 Bayesian inversion requires advanced computational tools like Markov Chain  
 84 Monte Carlo methods (MCMC) to sample from the posterior distributions  
 85 [Metropolis et al., 1953], [Chib and Greenberg, 1995], [Robert and Casella, 2013]. For  
 86 a tutorial on the class of MCMC algorithms classically used for Bayesian inversion (the  
 87 Metropolis-Hastings algorithm) the reader is referred to [Klauenberg and Elster, 2016].  
 88 Recently, Bayesian calibration using in-situ measurements has been widely used for  
 89 the inference of thermal properties and their associated uncertainties. To cite a few,  
 90 [Berger et al., 2016] tackled the estimation the thermal conductivity and the internal  
 91 convective heat transfer coefficient of a wall with 3 layers from one year experimental  
 92 data, [Iglesias et al., 2018] addressed the estimation of the thermal resistance and the  
 93 heat capacity of unit area of a homogeneous wall based on 7 days of measurements,  
 94 [Thébault and Bouchié, 2018] considered the estimation of the HLC with the ISABELE  
 95 method, [Simon et al., 2018] tackled the estimation of the thermal conductivity and the  
 96 heat capacity of the wall based on 8 days measurement campaign, [Rodler et al., 2019]  
 97 addressed the estimation of the thermal conductivity and the volumetric heat capacity  
 98 from a few days measurements.

99 This paper focuses on uncertainty propagation in inversion models. A widespread  
 100 approach is to consider input uncertainty sources as negligible or small enough to be  
 101 aggregated with uncertainties on the outputs [Perrin and Durantin, 2019]. Such an  
 102 approach is followed e.g. in [Simon et al., 2018] and [Berger et al., 2016]. However,  
 103 if the input uncertainties are not negligible or even if there is no information about  
 104 these input uncertainties, ignoring these uncertainties may result in biased estimated  
 105 calibration parameters [Perrin and Durantin, 2019]. The difficulty that arises for  
 106 uncertainty propagation is that there is usually no close functional form to describe  
 107 the relation between the uncertainty sources and the estimate of the calibration

108 parameters [Wang and Zabararas, 2004]. Many approaches have been developed to  
109 create approximate relationships through which uncertainties are propagated. An  
110 example of uncertainty propagation using the variance-covariance matrix of estimated  
111 parameters with the ordinary least squares (OLS) method and a (thermal) model  
112 reduction can be found in [François et al., 2020]. The analytical expression of  
113 the outputs in function of the initial and the boundary conditions, e.g. using  
114 discretized heat transfer equations as in [Iglesias et al., 2018] provides the "missing"  
115 relationship between the uncertainty sources and the estimates of the calibration  
116 parameters (obtained as Bayesian estimates of non linear regression parameters  
117 in [Iglesias et al., 2018]). [Thébault and Bouchié, 2018] and [Gori and Elwell, 2018]  
118 establish posterior relationships between the estimated parameters taken as the  
119 maximum a posteriori (MAP) and the uncertain inputs (e.g. posterior profile at MAP).  
120 Although the Bayesian approach conceptually allows to take into account measurement  
121 uncertainty in both inputs and outputs, [Perrin and Durantin, 2019] point out that little  
122 work has been done to uncertainties on inputs. The recent work by [Rodler et al., 2019]  
123 combines Metropolis-Hastings with Monte Carlo sampling from the uncertainty sources  
124 in an attempt of full Bayesian inversion.

125 The goal of the paper is to provide guidance on input uncertainty propagation in  
126 Bayesian inversion for the in-situ estimation of thermal parameters from temperature  
127 and flux measurements using a 1D thermal model. In this paper, we assume that  
128 the steps of review of the uncertainty sources, selection of the most influential and  
129 finally the prior quantification and modeling of uncertainty attached to all of them  
130 has been done before performing the Bayesian uncertainty analysis of the inversion  
131 problem. We show that uncertainty propagation of the experimental conditions through  
132 the inversion model can be performed by a fully Bayesian analysis of the inversion  
133 problem by posterior sampling from the joint prior distribution of the calibration  
134 parameters and the uncertain experimental conditions, following an approach similar to  
135 [Demeyer et al., 2021] and [Higdon et al., 2004]. The results are calculated with Markov  
136 Chain Monte Carlo methods (MCMC) and an introduction to these methods is given.

137 Among the various simulation studies [Ha et al., 2020] and experimental works  
138 carried out within the RESBATI project, the use case of this paper focuses on the  
139 thermal measurements obtained on a IWI (Inner Wall Insulation) test wall built within  
140 the project and circulated between LNE and CSTB. Here, we compare results from  
141 the Bayesian analysis of the thermal measurements obtained in an energy room at  
142 LNE with the results from the steady-state guarded hot box method at CSTB and we  
143 perform a sensitivity analysis to study the effect of measurement duration and the level  
144 of uncertainty.

145 **2. Bayesian calibration under uncertainty**

146 *2.1. General formulation*

147 Denoting  $y = (y_1, \dots, y_N)$  the vector of output measurements,  $X = (X_1, \dots, X_N)$  where  
 148  $X_i = (X_{i1}, \dots, X_{id})^T$ , the  $N \times d$  matrix of uncertain input variables and  $\theta$  the vector of  
 149 calibration parameters, the fully Bayesian inversion model writes

$$y = \eta(X, \theta) + \varepsilon \tag{1}$$

$$X \sim \pi(X) \tag{2}$$

$$\theta \sim \pi(\theta) \tag{3}$$

150 where  $\eta(X, \theta) = (\eta(X_1, \theta), \dots, \eta(X_N, \theta))$  denotes the vector of simulation outputs,  $\varepsilon =$   
 151  $(\varepsilon_1, \dots, \varepsilon_N)$  denotes the vector of output measurement error,  $\pi(X)$  and  $\pi(\theta)$  denote  
 152 respectively the prior distributions of  $X$  and  $\theta$ .

The unknown vector  $X$  is classically represented with an error in variable model (see  
 [Perrin and Durantin, 2019]) as a deviation from a known central value  $x$  (see discussion  
 section 2.5)

$$X = x + \zeta \tag{4}$$

153 where  $\zeta = (\zeta_1, \dots, \zeta_N)$  denotes the matrix of input measurement error and  $x = (x_1, \dots, x_N)$   
 154 denotes the matrix of input observations.

155 The random variables  $\varepsilon_i$  and  $\zeta_i$ , for  $i = 1, \dots, N$ , are commonly modeled as centered  
 156 Gaussian variables with known covariance matrix denoted  $\Sigma_\varepsilon$  and  $\Sigma_\zeta$  respectively  
 157 [Perrin and Durantin, 2019]. Furthermore  $\theta$ ,  $\varepsilon$  and  $\zeta$  are assumed statistically  
 158 independent.

159 *2.2. Modeling excess variance*

160 Model (1) assumes that output observations are equivalent to the calibrated simulations,  
 161 their difference being explained by the reported measurement uncertainties. In practice,  
 162 an excess variability of the  $y_i$  with respect to (w.r.t.) the variability explained by the  
 163 measurement uncertainty may be observed. Under the assumption that the simulator  
 164 is fit for purpose, not taking into account excess variance may lead to biased estimates  
 165 of the calibration parameters.

Under the hypothesis that the excess variability is due to a missing term in  
 the uncertainty budget ‡, we propose to model the excess variability (also called  
 heterogeneity of data) with an adjustment factor  $\sigma > 0$  as in [Bodnar and Elster, 2014]  
 and [Mana et al., 2012]

$$y = \eta(X, \theta) + \sigma\varepsilon \tag{5}$$

‡ In this paper, we assume that the excess variability of the time-varying thermal measurements  $y_i$   
 where  $i$  indexes time, comes from a missing influential source of uncertainty or from varying, not  
 controllable, conditions during the recording period (noise).

166 The parameter  $\sigma$  is related to the Birge ratio, that is often used in metrology to  
 167 enlarge quoted uncertainties when combining inconsistent measurement results on the  
 168 same measurand [Bodnar and Elster, 2014]. As shown in [Mana et al., 2012], the Birge  
 169 ratio can be interpreted as the most probable value of such an adjustment factor.

According to [Bodnar and Elster, 2014], it can be assumed that  $\sigma^2$  follows a priori  
 an inverse chi-squared distribution  $\sigma^2 \sim \text{InvChi}^2(\nu_0, s_0^2)$ , in which case the marginal  
 distribution of observations w.r.t  $\sigma^2$  is multivariate t-distributed

$$y \sim t_{\nu_0}(\eta(X, \theta), s_0^2 \Sigma_\varepsilon) \quad (6)$$

170 A poorly informative prior for  $\sigma^2$ , centered on 1, can be obtained with  $\nu_0 = 2$  and  
 171  $s_0^2 = 2$ .

### 172 *Remarks*

- 173 • The prior degree of freedom  $\nu_0$  can be viewed as allowing "uncertainty on the  
 174 uncertainty" contained in  $\Sigma_\varepsilon$  which comes to considering reported uncertainties as  
 175 point estimates of the unknown standard deviations.§ The assumption that the  
 176 missing source of uncertainty is common to all measurements translates into  $\nu_0$   
 177 being common to all measurements.
- 178 • Additive random effects || could be used to model excess variance if measurement  
 179 results  $y_i$  were obtained from uncertainty analyses performed independently, for  
 180 instance by various teams or with different measurement devices. They have become  
 181 common practice for instance when building consensus estimates in meta-analysis  
 182 and interlaboratory comparisons [Bodnar et al., 2017]. For such applications,  
 183 individual degrees of freedom  $\nu_i$  are taken into account when they are available,  
 184 see [Toman and Possolo, 2009].

### 185 *2.3. Bayesian inference*

186 In order to perform a full Bayesian analysis of the inversion problem, calibration  
 187 parameters  $\theta$  are augmented with the latent variables  $X$  and the heterogeneity variance  
 188 parameter  $\sigma^2$ . The Bayes formula provides the joint posterior distribution for  $(\theta, X, \sigma^2)$

$$\pi(\theta, X, \sigma^2 | y) \propto l(y | \eta(X, \theta), \sigma^2) \pi(\theta) \pi(\sigma^2) \pi(X) \quad (8)$$

§ For instance, the GUM uses the so-called Welch-Satterthwaite formula to estimate the degrees of  
 liberty associated with a measurement result assuming it is t-distributed.

|| The conventional random effects model considers the following model for the output observations

$$y = \eta(X, \theta) + \lambda + \varepsilon \quad (7)$$

where  $\lambda = (\lambda_1, \dots, \lambda_N)$  gathers for instance the team effects under the assumptions that  $\lambda_i \sim_{iid} N(0, \sigma^2)$ ,  
 $\varepsilon_i \sim N(0, u_i^2)$  and that the  $\lambda_i$  and the  $\varepsilon_i$  are independent.

189 where  $l(y|\eta(X, \theta), \sigma^2)$  is the likelihood,  $\pi(\theta)$ ,  $\pi(\sigma^2)$ ,  $\pi(X)$  are the prior distributions of  
 190  $\theta$ ,  $\sigma^2$  and  $X$  respectively, assumed independent. The prior distribution  $\pi(\theta)$  is usually  
 191 based on expert knowledge or tabulated values. The prior distribution for  $\sigma^2$  can be  
 192 chosen as poorly informative when the dataset is large. In order to account for the input  
 193 uncertainty sources  $X$ ,  $\pi(X)$  is a data-driven prior distribution based on (4).

194 In this paper, the quantity of interest is the joint posterior distribution  $\pi(\theta, X|y)$   
 195 obtained by integrating the joint posterior distribution out  $\sigma^2$

$$\pi(\theta, X|y) = \int_0^{+\infty} \pi(\theta, X, \sigma^2|y) d\sigma^2 \quad (9)$$

196 For a well-chosen prior distribution  $\pi(\sigma^2)$ , a closed form expression can be computed  
 197 for (9). For instance, using  $\sigma^2 \sim \text{Inv} - \text{chi2}(\nu_0, s_0^2)$  yields

$$\pi(\theta, X|y) \propto \pi(\theta)\pi(X)l_{int}(y|X, \theta) \quad (10)$$

198 where  $l_{int}(y|X, \theta) = t_{\nu_0}(\eta(X, \theta), s_0^2 \Sigma_\varepsilon)$

#### 199 2.4. Posterior simulation with Markov Chain Monte Carlo algorithms

200 Integrals (8), (9) or (10) are usually intractable and require simulation methods like  
 201 Markov Chain Monte Carlo (MCMC) methods. MCMC methods provide a flexible and  
 202 powerful tool for sampling from an arbitrary distribution. These methods construct a  
 203 sequence of dependent values which form a Markov chain with stationary distribution  
 204 equal to the sought posterior distribution. The Metropolis-Hastings (MH) algorithm  
 205 [Metropolis et al., 1953], [Chib and Greenberg, 1995] constitutes a popular class of  
 206 MCMC methods. The interesting feature of the MH algorithm is that it only requires to  
 207 know the posterior distribution up to a proportionality constant, i.e. the right-hand part  
 208 of Eq.8 or Eq.10, which makes it particularly suited for calibration problems. The MH  
 209 algorithm can be used in conjunction with the Gibbs algorithm if conditional posterior  
 210 distributions are tractable for a subset of parameters (the so-called *Metropolis-within-*  
 211 *Gibbs* algorithm). The sequence of values is considered after a burn-in period and often  
 212 the chains are thinned (i.e. only each 10th value is used) to decrease the autocorrelation  
 213 of the chains.

The Metropolis Hastings algorithm for sampling from the posterior distribution  
 of  $(\theta, X)$  given  $y$  in (10) is given in algorithm (1). The *initialization* step (line  
 1) provides a starting point for the iterative algorithm which can be sampled  
 from the prior distributions or near a best physical point if available or obtained  
 from computational techniques based e.g. on the gradient (Lagrange,...). At each  
 iteration  $l$ , a (multidimensional) *candidate*  $(\theta^{(c)}, X^{(c)})$  is sampled (line 5) and the  
 corresponding output of the thermal simulation  $\eta(\theta^{(c)}, X^{(c)})$  is computed (line 6). The  
*acceptance/rejection* step lines 8, 9 and 10 is based on the ratio of posterior distributions



(known up to the same constant, that disappears in the ratio)

$$\alpha = \frac{\pi(\theta^{(c)}, X^{(c)}|y)}{\pi(\theta^{(l-1)}, X^{(l-1)}|y)} \quad (11)$$

214 A candidate point with ratio  $\alpha < 1$  has probability  $\alpha$  to be selected which  
 215 corresponds to  $P(u < \alpha)$  where  $u \sim Unif(0, 1)$ . If a candidate is accepted, the candidate  
 216 is the new point of the chain, otherwise the previous point is added to the chain. It is  
 217 important to note that at each iteration an element is added to the chain, being either  
 218 the candidate or the previous point. For computational reasons, the log-posteriors are  
 219 used (line 2 for the log-posterior of the starting point and line 7 for the log-posterior of  
 220 the candidate point).

---

**Algorithm 1** Metropolis-Hastings algorithm for Bayesian calibration under uncertainty

---

**Input:** measurements  $x_i, y_i, t_i$  ;

**Output:**  $M$  samples from the posterior distribution  $\pi(\theta, X|y)$  according to (10);

- 1: initialize:  $(\theta^{(1)}, X^{(1)}, \eta^{(1)} = \eta(X^{(1)}, \theta^{(1)}))$ ;
  - 2: compute  $a = \ln(\pi(\theta^{(1)}, X^{(1)}|y))$ ;
  - 3: **repeat**
  - 4:    $l \leftarrow l + 1$ ;
  - 5:   sample  $\theta^{(c)} \sim N_d(\theta^{(l-1)}, \Sigma_\theta^{(l-1)})$  and  $X^{(c)} \sim N_N(X^{(l-1)}, \Sigma_X^{(l-1)})$  ;
  - 6:   generate  $\eta^{(c)} = \eta(X^{(c)}, \theta^{(c)})$  ;
  - 7:   compute  $b = \ln(\pi(\theta^{(c)}, X^{(c)}|\eta^{(c)}))$ ;
  - 8:   let  $\alpha = \min(\exp(b - a), 1)$  and  $u \sim Unif(0, 1)$ ;
  - 9:   if  $\alpha \geq u$  then  $\theta^{(l)} = \theta^{(c)}$  and  $X^{(l)} = X^{(c)}$ ;
  - 10:   else  $\theta^{(l)} = \theta^{(l-1)}$  and  $X^{(l)} = X^{(l-1)}$ ;
  - 11:    $a \leftarrow b$
  - 12: **until**  $l = M$
- 

## 221 2.5. Discussion

222 The Bayesian approach allows a flexible modelling of the prior distributions  $\pi(X)$   
 223 and  $\pi(\theta)$  due to the use of MCMC simulation methods, among which the Gaussian,  
 224 Student, rectangular, triangular and trapezoidal distributions that are commonly  
 225 used to represent uncertainty on input quantities e.g. in metrology (see GUM-  
 226 S1 [BIPM et al., 2008b]). For instance, the Gaussian distribution can be used  
 227 to model inputs resulting from an uncertainty propagation (e.g. following the  
 228 GUM propagation of variance [BIPM et al., 2008a]) like the solar aperture and the  
 229 volumetric flowrate. Generally, the prior on  $\theta$  consists in a rectangular distribution  
 230 defining bounds inside which the unknown value is supposed to lie, to improve  
 231 the computational efficiency of the inversion method. For example, the bounds  
 232 associated with thermophysical properties of material can usually be found in literature

233 [Heo et al., 2012], [ASHRAE, 2017]. More generally, guidelines for assessing the  
234 uncertainty of inputs used in building energy models can be found in [Macdonald, 2002]  
235 and [Heo et al., 2012].

236 To account for complex uncertain inputs like those related to time (e.g.  
237 occupancy, weather, usage...), a discrepancy term  $\delta(x)$ , function of these inputs, is  
238 usually added to (1) [Heo et al., 2012] and  $\pi(X)$  is modeled as a Gaussian Process  
239 [Rasmussen and Williams, 2006], [Santner and Notz, 2003]. A complete Bayesian  
240 framework for modelling an additional discrepancy term in inversion is proposed in  
241 [Higdon et al., 2004], [Kennedy and O’Hagan, 2001]. In this paper, due to the active  
242 method, temperature and flux measurements are likely to be non-stationary time  
243 processes that would require modeling using e.g. Gaussian processes functions of both  
244  $x$  and  $y$ . For simplicity, we choose to model the uncertain time varying inputs and  
245 outputs following (4) and (1) respectively and to leave the thorough modeling of input  
246 and output time series and their associated uncertainties in Bayesian inversion as a  
247 perspective of this work. Indeed, for the analysis of the real case study, such further  
248 work did not prove necessary.

249 In this paper, we propose a fully Bayesian approach of inversion problems to  
250 propagate uncertainties of input parameters during the inversion procedure, which comes  
251 to treat all parameters as *calibration parameters* in classical Bayesian inversion. Such  
252 an approach is even recommended as a baseline of any Bayesian inversion procedure in  
253 [Higdon et al., 2004]. Indeed, according to [Higdon et al., 2004], even if we believe that  
254 the true physical value is known, allowing a slight deviation from the true physical value  
255 (similar to representation (4)) may produce an empirically better model of the reality.  
256 Furthermore, estimations of the calibration parameters may not even be interpreted as  
257 estimates of the true physical values of these parameters [Higdon et al., 2004]. Rather,  
258 they are by nature a ’best fit’ estimate of  $\theta$  depending on the many hypotheses (among  
259 which that the thermal model is a perfect fit of the physical phenomenon) and the  
260 experimental conditions involved in the whole process.

261 In this paper, the use of an active method on a short period (24 hours) allows to limit  
262 bias due to the sensitivity of the inversion procedure to the environmental conditions.  
263 Indeed, the effect of occupancy, weather and usage are potentially the most influential  
264 on the measure of thermal parameters (or more generally the energy performance) but  
265 also the most uncertain [Goffart et al., 2017]. If any, model approximation (assumed  
266 small) is taken into account in the free variance parameter  $\sigma^2$  used to capture the excess  
267 variance with respect to the reported uncertainties, with the aim of limiting bias of the  
268 estimated calibration parameters due to modeling.

### 269 **3. Application to the in-situ estimation of the thermal resistance of a wall**

#### 270 *3.1. Motivation and context*

271 The thermal resistance  $R$  ( $\text{m}^2 \text{K W}^{-1}$ ) of the envelope of a building is an indicator of  
272 the thermal performance of the building. Within the RESBATI project, a measurement  
273 method of the thermal resistance of opaque walls has been developed to produce in-situ  
274 results with an associated uncertainty in less than three days.

275 In order to evaluate the performance of the method, a test wall of dimensions 2  
276 meters by 2 meters with inner wall insulation (IWI) was built. The insulation layer  
277 is made of EPS (expanded polystyrene). In this application, we compare the results  
278 obtained by the active method on the test wall placed in an energy room at LNE, France  
279 (see sections 3.2 and 3.5.3), with results obtained with the steady-state guarded hot box  
280 method [ISO 8990:1994, 1994] at CSTB, France (see section 3.5.2). For this application,  
281 the steady-state guarded hot plate method [ISO 8302:1991, 1991] (see section 3.5.1) is  
282 used to estimate the thermal resistance of the insulation layer (EPS). The description  
283 of the experimental conditions of each method is given.

#### 284 *3.2. Description of the energy room REBECCA at LNE*

285 The energy room at LNE is a climatic chamber inside another climatic chamber. It  
286 is composed of an internal cell with the dimensions of a dwelling (3.42 m of side on  
287 2.29 m high, surface of the test specimen  $7.83 \text{ m}^2$ ). The latter is surrounded by 4  
288 climatic chambers in which it is possible to modify the temperature between  $-7^\circ\text{C}$   
289 and  $35^\circ\text{C}$  and to generate any type of transient regime (hot cold, cycle, etc.). The  
290 four surrounding boxes (front cell, guard, floor and ceiling) can be controlled separately  
291 (Figure 2). The REBECCA (Research and Testing of Buildings and Heat Emitters  
292 under Artificial Climate) cell is built to reproduce the principle of a guarded hot box  
293 test but with more room inside to install additional devices. The front panel is equipped  
294 with the specimen to be studied. In order to ensure that the entire heat flow passes  
295 through the test specimen, the 5 walls of the inner cell in contact with the thermal guard  
296 are insulated with Vacuum Insulated Panels having a thermal resistance greater than  
297  $10 \text{ m}^2 \text{K W}^{-1}$ . The test can be carried out under steady state condition, which occurs  
298 after a long period of time, or in a transient way like temperature ramp.

#### 299 *3.3. Description of the measurement process with the active method*

300 The test wall is installed in the REBECCA cell and an active method is used to produce  
301 faster in-situ results using a heating module, temperature and flux sensors placed on  
302 the wall, as displayed in Figure 3.

303 The active method uses a prototype built by the laboratory CERTES (Centre  
304 d'Études et de Recherche en Thermique, Environnement et Systèmes, Université Paris  
305 Est Créteil, France) within the RESBATI project. The prototype is a cube of 60 cm  
306 of side. One side is open; in the opposite side 24 DC halogen spots of 20 W are

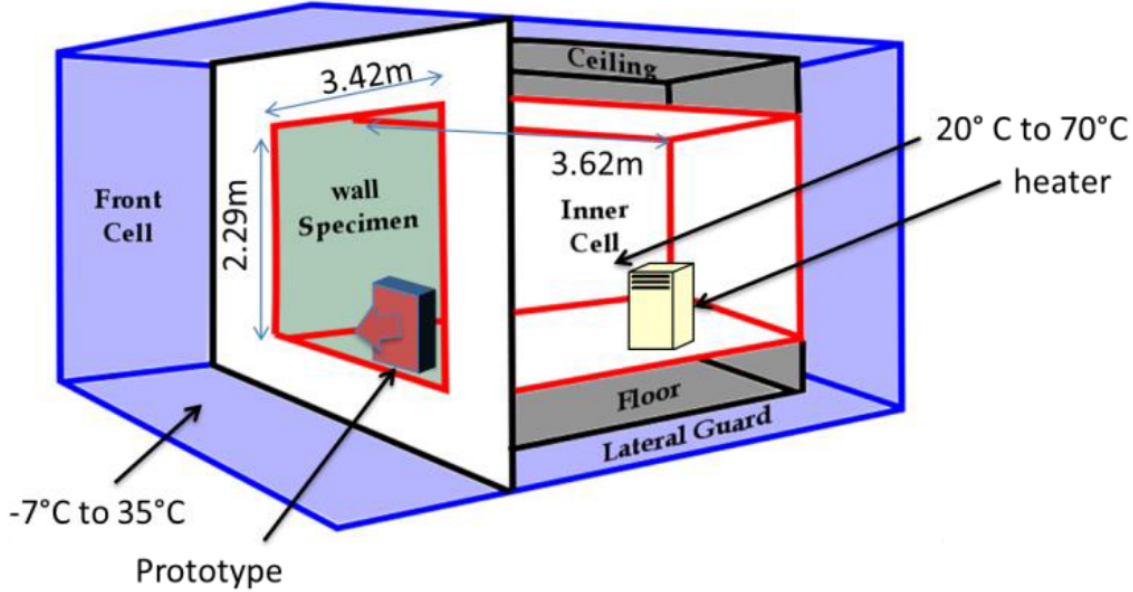


**Figure 2.** Schematic diagram of the energy room called 'REBECCA' at LNE, France, from [Koenen et al., 2019].

307 positioned. The maximum electrical power is 480 W that can be adjusted depending on  
 308 the test scenario. The four remained faces are insulated with reflective material with  
 309 a low emissivity. In the front side in contact with the IWI, a heat flow meter with  
 310 thermocouples is positioned. The IWI is then heated by the halogen spots. The heat  
 311 flow that goes in the wall through the heat flow sensor and the surface temperatures of  
 312 the wall are measured every 2 s. A step heating excitation which can reach several days  
 313 is used for all experiments. A schematic description and a view of the experimental set-  
 314 up are presented in Figure 3 and Figure 4. A number of 30 thermocouples are positioned  
 315 along the heat flow meter to validate the one dimension hypothesis.

316 The heat flow sensors were calibrated in the LNE guarded hot plate at different  
 317 mean temperatures  $T$  (mean of external and internal temperatures) and temperature  
 318 difference  $\Delta T$  between the internal and external temperatures. All thermocouples were  
 319 calibrated at LNE. A test lasts 24 h after steady state condition is achieved. This can  
 320 continue several days depending on the thermal properties of the walls.

321 The RESBATI device induces a constant power of 105 W. The external cell was  
 322 cooled at 0 °C and the internal room was heated at 20 °C in order to obtain a temperature  
 323 difference  $\Delta T$  of 20 °C between the two sides of the wall. The heat flow going through  
 324 the wall in the RESBATI area is measured continuously and reaches around  $10 \text{ W m}^{-2}$   
 325 after 10 h and remains constant afterwards.

326 In this application, the standard uncertainty (evaluated at LNE) associated with the  
 327 inner and outer surface temperatures ( $T_{si}$  and  $T_{se}$  respectively) is  $u(T_{si}) = u(T_{se}) =$   
 328  $0.5 \text{ °C}$  and the standard uncertainty associated with the absorbed flux  $q_{int}$  is  $u(q_{int}) =$

329  $3\%q_{int} \text{ W m}^{-2}$ .

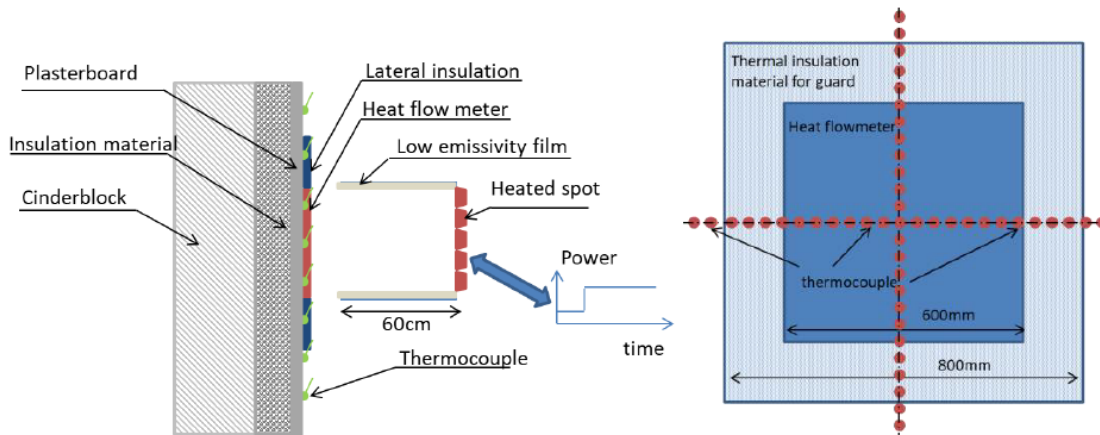


**Figure 3.** Schematic view of the experimental setup (side view, face view), from [Koenen et al., 2019].

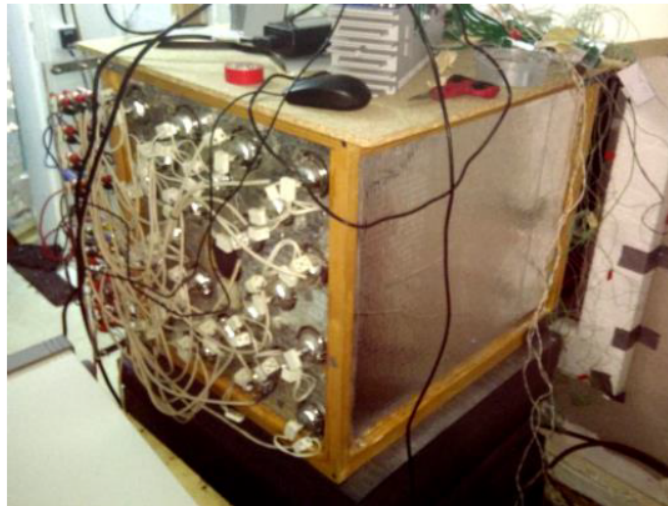


**Figure 4.** View of the active method prototype, from [Koenen et al., 2019].

330 The thermal resistance of a multi-layer wall is measured indirectly from temperature  
 331 and flux measurements after the identification of the parameters  $\theta$  of a thermal model  
 332  $\eta(X, \theta)$  (here with  $X = (T_{se}, q_{int})$ , see section 3.4) using the Bayesian approach  
 333 described section 2. A 1D transient thermal model solved with a finite element  
 334 method in space and a Euler implicit time integration scheme was chosen in this  
 335 study that takes the heat capacity of unit area  $cw_i$  ( $\text{J m}^{-2} \text{K}^{-1}$ ) and the thermal  
 336 conductivity  $k_i$  ( $\text{W m}^{-1} \text{K}^{-1}$ ) of each layer  $i$  as calibration inputs gathered in the vector  
 337  $\theta = \{cw_i, k_i\}_{i=1, \dots, I}$  where  $I = 4$  is the number of layers.

The thermal resistance of the wall is expressed as the sum of the thermal resistance

$R_i$  of each layer

$$R = \sum_{i=1}^I R_i, \text{ with } R_i = \frac{l_i}{k_i} \quad (12)$$

where  $l_i$  (m) is the thickness of layer  $i$  (in this study,  $l_i$  is considered known, see values in Table 7). The estimate of the thermal resistance and its associated uncertainty are obtained with the Monte Carlo method applied to (12) using the samples from the posterior distributions of the  $k_i$ . In particular,  $R_2$  denotes the thermal resistance of the insulation layer.

*Comments on the identifiability of the thermal parameters* With this choice of thermal model and the low number of used sensors, we numerically observe that only the joint distribution of the input thermal parameters is identifiable but not its individual constituents (various combinations of values for  $cw_i$  and  $k_i$  could produce close thermal resistance values). This is a common situation in inversion problems, see the point of [Higdon et al., 2004] discussed in section 2.5, which is overcome here by considering that the thermal resistance (here, the quantity of interest) is identifiable but *a priori* not the  $cw_i$  and  $k_i$  taken individually. It is thus important to take samples from the joint posterior distribution to perform the Monte Carlo estimation of the thermal resistance.

Still, from virtual testing and model-based sensitivity analysis, the thermal conductivity of the insulation layer  $k_2$  should be identifiable for this application. Thus, the comparison of the posterior distribution of  $k_2$  with an experimental result (e.g. obtained with GHP) could be used as an indication of the ability of the method to estimate the thermal resistance of the insulation layer (calculated as  $R_2 = l_2/k_2$ ), see section 3.5.3. Besides, in this study, the thickness of the layers of the wall is assumed to be known, but in general the thickness should be estimated as well with prior knowledge e.g. based on approximate measurements or from the design of the wall. More generally, identifiability issues are tackled with the use of informative prior distributions.

### 3.4. Review of uncertainty sources to specify $X$

In order to perform a sound uncertainty analysis, the first step is to deeply analyse the measurement process by performing the most exhaustive review of the uncertainty sources pertaining to it (even those that are not quantifiable). This is a demanding brainstorming step involving both experts of the field and statisticians. The classical tool for such a task is the Ishikawa diagram, which is used in the GUM [BIPM et al., 2008a] to review the sources of uncertainty involved in a measurement process.

Figure 5 displays an instance of an Ishikawa diagram pertaining to the measurement process of the thermal resistance of a wall using the RESBATI prototype. Uncertainty sources are divided into five categories shortly described thereafter.

**Means:** refers to all the uncertainty sources involved with the measurements (sensors, reference materials, standards), here limited to sensors;

373 **Method:** refers to all uncertainty sources related to the measurement procedure and  
 374 the data analysis which consists here in an identification method;

375 **Wall/Enveloppe:** refers to the object of the measurement, here the wall; for this  
 376 application, the thermo-physical properties are the calibration parameters of the  
 377 thermal model (see Figure 1);

378 **Environment:** refers to the variations of the experimental conditions during the  
 379 process, here in the energy room;

380 **Operator:** refers to the uncertainty arising from the interpretation and the  
 381 implementation of the procedure by operators involved in the whole process.

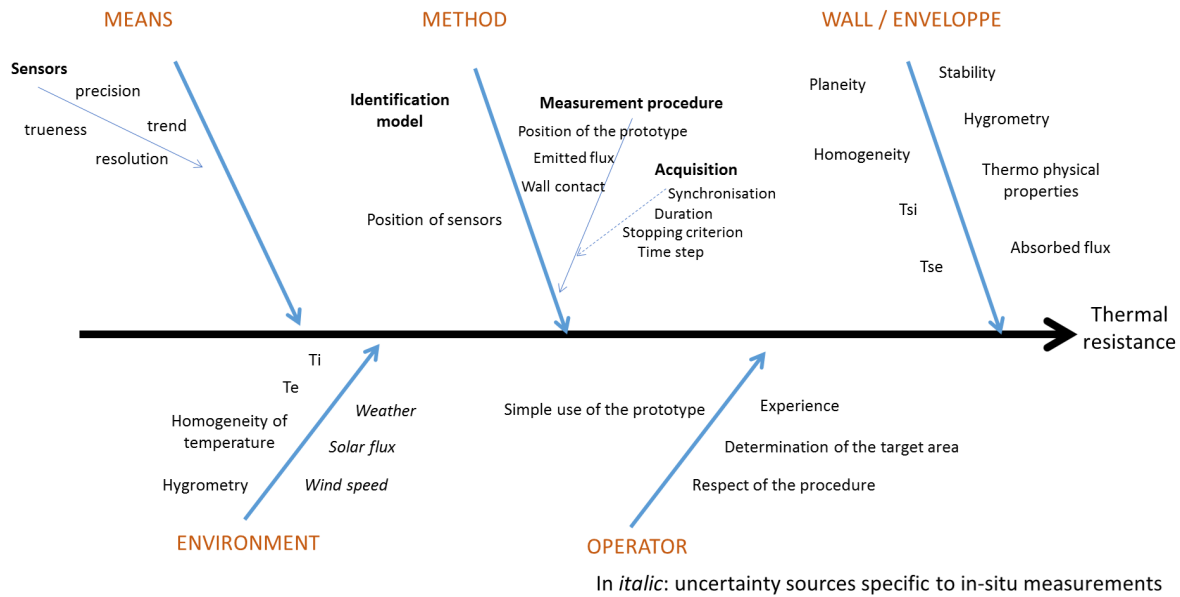


Figure 5. Ishikawa diagram for the thermal resistance.

382 Figure 6 describes the uncertainty sources pertaining to the identification model i.e  
 383 to the thermal model and the inversion procedure.

384 In practice, only the most influential quantifiable uncertainty sources  $X$  are kept  
 385 for the uncertainty analysis. Such a selection can be performed with sensitivity  
 386 analysis methods [Saltelli et al., 2004] and/or by experts based on prior knowledge  
 387 or information. It is important to note that the combined effect of unquantifiable  
 388 uncertainty sources, assumed to vary randomly when repeating measurements, can be  
 389 taken into account when processing measurements.

390 Here, we choose to focus only on  $X = (T_{se}, q_{int})$  as an example of uncertainty  
 391 propagation associated with temporal measurements.

### 392 3.5. Results for IWI test wall

393 In this section, we compare the estimates of the thermal resistance of the IWI wall  
 394 obtained with the active method using the Bayesian inversion under uncertainty with

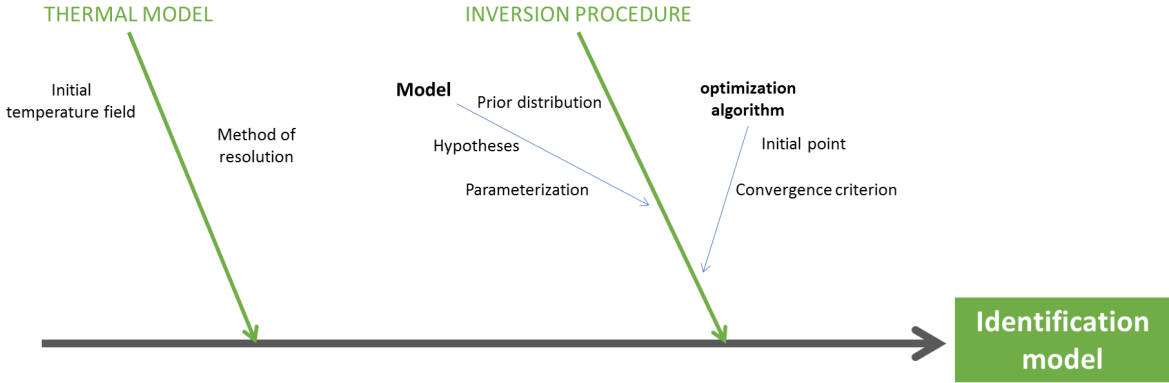


Figure 6. Ishikawa diagram for the identification model.

395 those obtained with the steady-state guarded hot box at CSTB, France in comparable  
 396 experimental conditions ( $T = 10\text{ }^\circ\text{C}$  and  $\Delta T = 20\text{ }^\circ\text{C}$ ). As discussed section 3.3, many  
 397 calibration parameters are not identifiable but the thermal conductivity of the insulation  
 398 material  $k_2$  should be identifiable. The comparison of the posterior distribution of  $k_2$   
 399 with the experimental result obtained by LNE using the guarded hot plate method is  
 400 also used as an indication of the performance of the Bayesian inversion method. Indeed,  
 401 the thermal resistance of the insulation layer (calculated as  $R_2 = l_2/k_2$ ) is far the most  
 402 important contribution to the global thermal resistance of the IWI wall. A sensitivity  
 403 study is performed to show the effect of duration and input uncertainties on the results  
 404 of the Bayesian inversion.

405 *3.5.1. Guarded hot plate results* The guarded hot plate apparatus [ISO 8302:1991, 1991]  
 406 determines steady-state thermal transmission properties of flat slab specimens having a  
 407 low thermal conductivity. It uses the one-dimensional steady-state thermal conductivity  
 408 equation. The relative standard uncertainty associated with GHP results is evaluated  
 409 around 0.5%.

410 To conduct the measurement, we have cut two specimen of  $600 \times 600$  mm from IWI  
 411 coming from the same batch than those used to build the test wall. The measurements  
 412 in the guarded hot plate were done at  $T = 10\text{ }^\circ\text{C}$  mean temperature and  $\Delta T = 15\text{ }^\circ\text{C}$ .  
 413 The result is computed as a mean over 8 hours after the steady state is reached. Results  
 414 are displayed in Table 1. Tabulated values for the plasterboard and the cinderblock are  
 415 given in Table 2.

416 *3.5.2. Guarded hot box results* The guarded hot box [ISO 8990:1994, 1994] assesses the  
 417 thermal performance of walls at full scale. The wall to be tested is positioned between  
 418 two ambient conditions: one hot and one cold. Here, the complete wall  $2 \times 2$  m was  
 419 measured in a GHB at CSTB, France at  $T = 10\text{ }^\circ\text{C}$  and  $\Delta T = 20\text{ }^\circ\text{C}$ . The result  
 420 is computed as a mean over 10 hours after the steady state is reached. Under these  
 421 conditions, the thermal resistance of the specimen wall using the GHB is given by the



Layer	Heat capacity of unit area $cw$ /J m <sup>-3</sup> K	Thermal conductivity $k$ /W m <sup>-1</sup> K <sup>-1</sup>	Thermal resistance $R$ /m <sup>2</sup> K W <sup>-1</sup>
EPS	$cw_2 = 1.35 \times 10^4$	$k_2 = 0.031$	$R_2 = 3.85$
EPS + Plasterboard	-	-	3.9

**Table 1.** Measured thermal performance on GHP.

Layer	Heat capacity of unit area $cw$ /J m <sup>-3</sup> K	Thermal conductivity $k$ /W m <sup>-1</sup> K <sup>-1</sup>	Thermal resistance $R$ /m <sup>2</sup> K W <sup>-1</sup>
Plasterboard	$cw_1 = 7.30 \times 10^4$	$k_1 = 0.250$	0.05
Cinderblock	$cw_3 = 9.25 \times 10^4$	$k_3 = 0.850$	0.2

**Table 2.** Tabulated thermal performance values.

422 95% coverage interval defined by  $4.08 \pm 0.86$  m<sup>2</sup> K W<sup>-1</sup>, see details in Appendix A.

423 *3.5.3. Active method coupled with Bayesian inversion* Measurements recorded every  
 424 two seconds for 24 hours are displayed in Figure 7 for the surface temperatures  $y = T_{si}$   
 425 and  $T_{se}$  and in Figure 8 for the absorbed flux  $q_{int}$  ( $X = (T_{se}, q_{int})$ ). It can be observed  
 426 that the absorbed flux becomes constant after 10 hours. For computational issues,  
 427 measurements are sampled every 300 seconds for a total of  $N = 289$  measurements.

428 A sensitivity analysis is performed to show the effects of duration and experimental  
 429 uncertainties on the estimation of both the thermal conductivity  $k_2$  of the insulation  
 430 layer (EPS) and the estimation of the global thermal resistance  $R$ .

431 Table 3 describes the three uncertainty configurations ("no input uncertainty",  
 432 "low level", "medium level") considered in the study. It is important to note that  
 433  $u(T_{si}) = u(T_{se})$  in all configurations due to the experimental setting. The case "no  
 434 input uncertainty" corresponds to the classical modelling where the input uncertainty  
 435 is not taken into account but the output uncertainty is set to its experimental value  
 436  $u(T_{si}) = 0.5$  °C. The case "low level input uncertainty" corresponds to the case where  
 437 all experimental uncertainties would have been underestimated. The case "medium  
 438 level uncertainty" corresponds to taking into account all the experimental values of  
 439 uncertainties provided by LNE. This configuration is recommended *a priori*.

440 The effect of duration is studied for the recommended "medium level of uncertainty"  
 441 and the effect of uncertainty is studied for the duration 24 hours. The resulting labels  
 442 used in the legends of Figures 9, 10 and 11, are displayed in Table 4.

443 To conduct the Bayesian analysis, uniform prior distributions are assigned to the  
 444 calibration parameters, whose bounds are displayed in Table 5. The resulting prior  
 445 for the thermal resistance is obtained with Monte Carlo simulations from (12) and  
 446 displayed as the grey histogram in Figure 10. The prior distribution for the excess

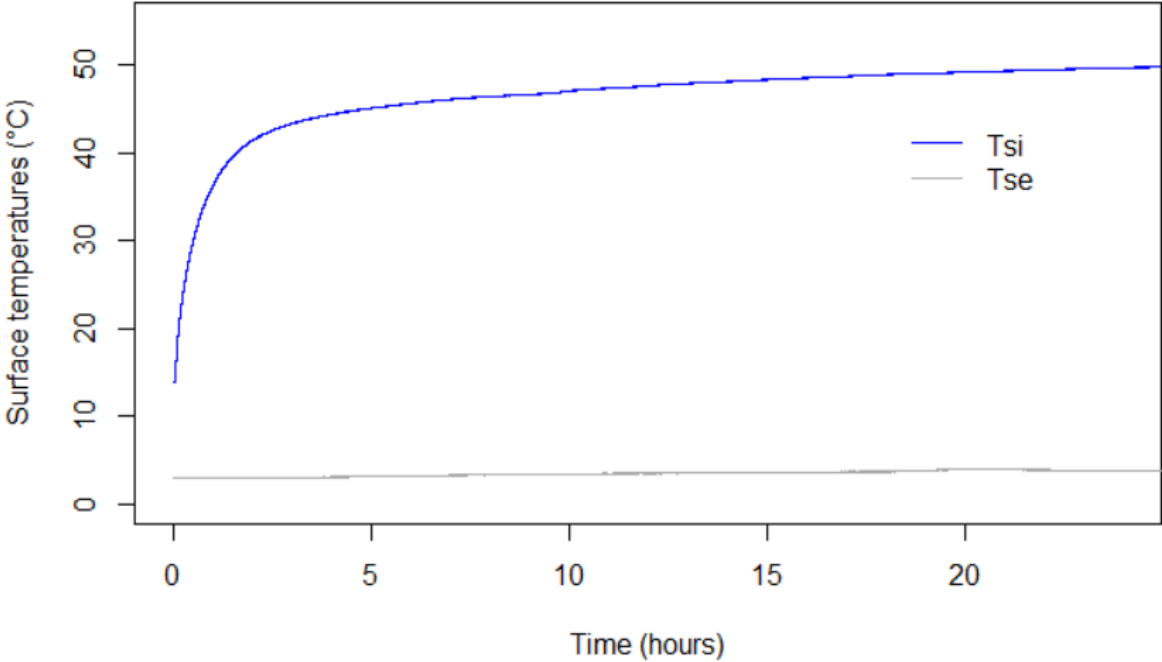


**Figure 7.** Surface temperature measurements for the IWI wall placed in the energy room REBECCA at LNE, France.

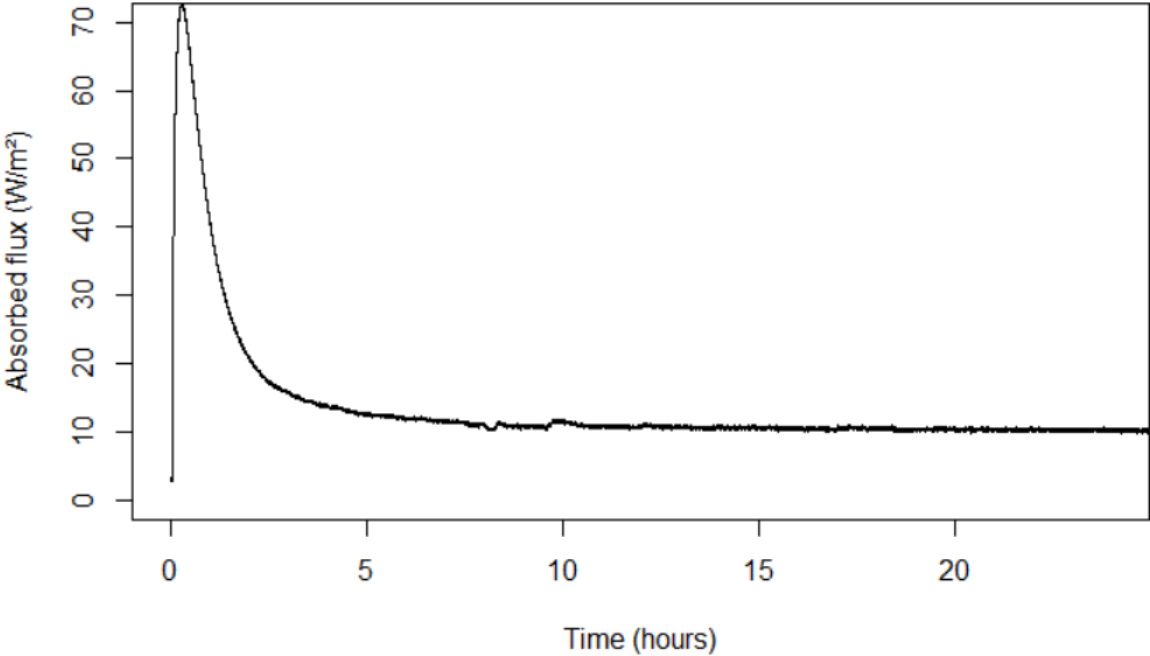


**Figure 8.** Absorbed flux measurements for the IWI wall placed in the energy room REBECCA at LNE, France.

447 variance parameter is chosen as  $\pi(\sigma^2) \sim \text{InvChi}^2(\nu_0, s_0^2)$  with  $\nu_0 = 2$  and  $s_0^2 = 0$  to make  
 448 it poorly informative as explained in section 2.2. Prior distributions of uncertain inputs  
 449 in the vector  $X = (Tse^T, q_{int}^T)^T$  are modeled following (4) with

$$\Sigma_\zeta = \begin{pmatrix} \Sigma_{Tse} & 0 \\ 0 & \Sigma_{q_{int}} \end{pmatrix} \quad (13)$$

450 where  $\Sigma_{Tse} = \text{diag}(\{u^2(Tse)\}_N)$  and  $\Sigma_{q_{int}} = \text{diag}(\{u^2(q_{int})\}_N)$  are the diagonal matrices  
 451 of dimension  $N \times N$  of reported variances of  $Tse$  and  $q_{int}$  respectively. Similarly, the  
 452 covariance matrix of output observations  $y$  is chosen diagonal as  $\Sigma_\epsilon = \text{diag}(\{u^2(Tsi)\}_N)$ .

453 The MCMC procedure described in Algorithm 1 was run for each case from Table  
 454 4 with 50000 iterations, a burn-in of 20000 iterations and a thinning of 30 iterations.  
 455 For each case, we controlled that the acceptance rate falls between 15% and 30%. For  
 456 the "no input uncertainty" case the number of parameters is 8 (number of calibration  
 457 parameters), whereas in the two other cases the propagation of input uncertainties  
 458 involves  $2N$  additional parameters corresponding to the elements of vector  $X$ , for a  
 459 total of 586 parameters.

Level of uncertainty	$u(Tsi)$ /°C	$u(Tse)$ /°C	$u(q_{int})$ /W m <sup>-2</sup>
no input uncertainty	0.5	-	-
low level	0.1	0.1	1% $q_{int}$
medium level	0.5	0.5	3% $q_{int}$

**Table 3.** Description of uncertainty configurations.

Level of uncertainty	Duration	
	12h	24h
no input uncertainty	-	24h_no_uncertainty
low level	-	24h_T001_Q1pct
medium level	12h_T005_Q3pct	24h_T005_Q3pct

**Table 4.** Labels used in the legends of plots resulting from the choice of duration and uncertainty configurations.

460 *Results for the thermal conductivity of the insulation layer (EPS, Expanded Polystyrene)*  
 461 Figure 9 shows the effect of duration on the estimation of the thermal conductivity  $k_2$   
 462 for the medium uncertainty level. The comparison with the guarded hot plate result  
 463 (GHP, see section 3.5.1) displayed as the black dashed Gaussian distribution shows that  
 464 the posterior estimate of  $k_2$  is biased for 12 hours whereas the posterior estimate for 24

Layer	Thickness /m	Thermal conductivity $k$ /W m <sup>-1</sup> K <sup>-1</sup>	Heat capacity of unit area $cw$ /J m <sup>-2</sup> K <sup>-1</sup>
Plasterboard	$l_1 = 0.013$	$0.2 \leq k_1 \leq 0.4$	$7 \times 10^5 \leq cw_1 \leq 8 \times 10^5$
EPS	$l_2 = 0.120$	$0.02 \leq k_2 \leq 0.04$	$1 \times 10^4 \leq cw_2 \leq 3 \times 10^4$
Cinderblock	$l_3 = 0.150$	$0.7 \leq k_3 \leq 1.2$	$8.5 \times 10^5 \leq cw_3 \leq 2 \times 10^6$
Exterior coating	$l_4 = 0.015$	$0.5 \leq k_4 \leq 1.2$	$1 \times 10^6 \leq cw_4 \leq 2 \times 10^6$

**Table 5.** Characterisation of each layer: thickness (assumed known in this application) and bounds for the uniform prior distributions of the thermal parameters, found in the literature.

465 hours is unbiased (the posterior distribution of  $k_2$  is centered on the GHP best estimate).  
 466 In other words, for 24 hours, the estimate of the thermal conductivity of the insulation  
 467 material ( $k_2$ ) is consistent with the physical value assessed with the guarded hot plate  
 468 method.

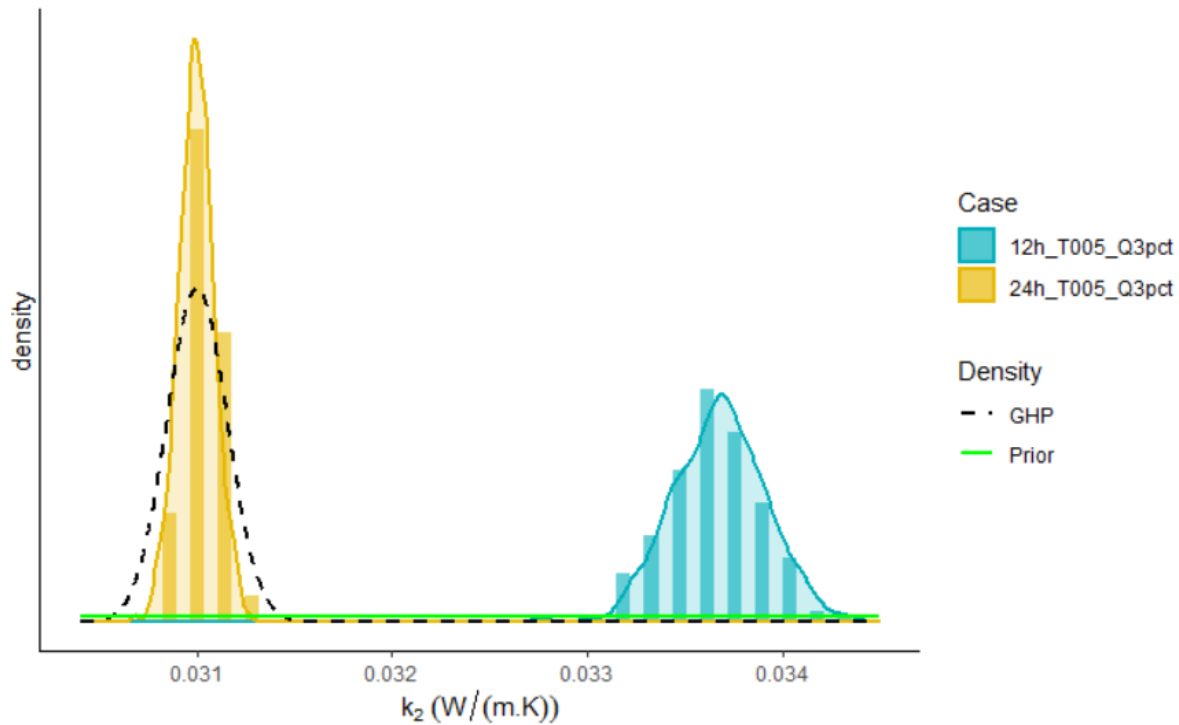


**Figure 9.** Histograms of the posterior samples for  $k_2$  obtained after 12 hours and 24 hours and plots of the Gaussian distribution associated with the guarded hot plate (GHP) result and the prior distribution.

469 Table 6 gives the posterior estimates for all the uncertainty configurations. It can  
 470 be observed that for 24 hours, all posterior results are consistent with the GHP  
 471 (the best estimate of the GHP 0.031 is included in the 95% Bayesian credible intervals).

472 It is important to note that the number of significant digits provided on the GHP  
 473 result does not allow to compare the posterior results in terms of bias because all rounded  
 474 posterior mean results are unbiased equal to 0.031. So the comparison with the GHP  
 475 result does not allow to study the effect of uncertainty but globally says that the Bayesian  
 476 methodology provides unbiased estimates of  $k_2$  (w.r.t GHP result) and then of  $R_2$  for a  
 477 24 h observation.

Duration /h	$u(T_{si})$ /°C	$u(T_{se})$ /°C	$u(q_{int})$ /W m <sup>-2</sup>	$\hat{k}_2$ /W m <sup>-1</sup> K <sup>-1</sup>	$u(\hat{k}_2)$ /W m <sup>-1</sup> K <sup>-1</sup>	Shortest 95% CI /W m <sup>-1</sup> K <sup>-1</sup>
24	0.1	-	-	0.0309	0.0001	[0.0307, 0.0311]
24	0.5	-	-	0.0309	0.0001	[0.0307, 0.0311]
24	0.1	0.1	1% $q_{int}$	0.0309	< 0.0001	[0.0307, 0.0310]
12	0.5	0.5	3% $q_{int}$	0.0337	0.0003	[0.0333, 0.0342]
24	0.5	0.5	3% $q_{int}$	0.0310	< 0.0001	[0.0308, 0.0312]

**Table 6.** Results of the sensitivity study for the thermal conductivity  $k_2$ .

478 *Results for the thermal resistance of the wall* Figure 10 displays the results for the  
 479 *global resistance of the wall* obtained with the guarded hot box method (GHB, see  
 480 section 3.5.2) represented by a Gaussian approximation with 95% coverage interval  
 481 (dashed vertical bars), the estimate of  $R_2$  from the GHP result (see Table 1) and its  
 482 95% coverage interval (in black) and the posterior estimates of the thermal resistance  
 483 and their associated 95% credible intervals (represented with horizontal turquoise and  
 484 yellow dashes) obtained with the active method for the medium level of uncertainty for  
 485 12 hours and 24 hours respectively. Note that the histogram plot of the prior distribution  
 486 shows that the prior  $u$  for the global thermal resistance of the wall is consistent with the  
 487 GHB result.

488 The 95% coverage interval for the GHB result covers all results (even those  
 489 incomplete for only 12 hours) which means that the comparison which the GHB result  
 490 cannot be used alone to evaluate the performance of the Bayesian method in the  
 491 various configurations. We can underline that active solicitation coupled with Bayesian  
 492 technique, which was developed for in-situ application, can lead to identification results  
 493 as accurate as those obtained in GHP.

494 The ability of the Bayesian method to provide an unbiased estimate of  $R_2$  was  
 495 demonstrated previously. Since  $R_2$  represents 95% of the expected global thermal  
 496 resistance  $R$ , the fact that the posterior estimate of the global resistance for 24 hours is  
 497 closed to the best estimate of the GHB makes highly credible the ability of the Bayesian  
 498 method to also provide an unbiased estimate of  $R$  for 24 hours.

499 The comparison with the *thermal resistance of the EPS*  $R_2$  obtained from the GHP  
 500 estimate of  $k_2$  (black line) also shows that the estimate of the thermal resistance obtained  
 501 after 12 hours (blue line) nearly allows to retrieve the thermal resistance of the EPS.

502 It is important to note that the comparison with the GHB result does not allow  
 503 to study finely the effect of uncertainty in terms of resulting bias on the global thermal  
 504 resistance.

505 Results of the sensitivity study in terms of the global thermal resistance are  
 506 displayed in Table 7. We observe that the posterior uncertainty is similar (with two  
 507 significant digits) for the configurations involving 24 hours records.

508 Finally, the plot of the posterior distribution of the thermal resistance of the wall for  
 509 24 hours and medium input uncertainty is displayed in Figure 11 with its 95% credible  
 510 interval.

511 *3.5.4. Remarks* For both experiments conducted in a climatic chamber with similar  
 512 controlled environmental conditions, the active method developed in the RESBATI  
 513 project allows to estimate the thermal resistance with a relative uncertainty of less  
 514 than 2% instead of 10% for the guarded hot box.

515 More generally, for in-situ measurements, the use of an active method should lessen  
 516 the influence of uncontrolled environmental conditions so that, in practice, the same  
 517 modelling should be used for in-situ measurements than for measurements obtained in  
 518 the climatic chamber. Precisely, a sharp modelling is not required for the complex input  
 519 quantities like weather, occupation,...

Duration /h	$u(T_{si})$ /°C	$u(T_{se})$ /°C	$u(q_{int})$ /W m <sup>-2</sup>	$\hat{R}$ /m <sup>2</sup> K W <sup>-1</sup>	$u(\hat{R})$ /m <sup>2</sup> K W <sup>-1</sup>	Shortest 95% CI /m <sup>2</sup> K W <sup>-1</sup>
24	0.1	-	-	4.064	0.014	[4.039, 4.091]
24	0.5	-	-	4.072	0.014	[4.045, 4.101]
24	0.1	0.1	1% $q_{int}$	4.083	0.014	[4.054, 4.107]
12	0.5	0.5	3% $q_{int}$	3.759	0.025	[3.712, 3.808]
24	0.5	0.5	3% $q_{int}$	4.058	0.014	[4.031, 4.087]

**Table 7.** Results of the sensitivity study for the global thermal resistance.

## 520 4. Conclusion and discussion

521 This paper presents a Bayesian approach for the indirect measurement of thermal  
 522 parameters of a wall from thermal measurements obtained with thermocouples and  
 523 fluxmeters using an active method. This work is part of the ANR RESBATI project  
 524 whose main objective is to develop a portable measurement device for evaluating the  
 525 thermal resistance of opaque building walls on site. The case study chosen in this paper  
 526 concerns the analysis of measurements performed on an internal wall insulation (IWI)  
 527 built within the project. The work takes advantage of the experimental work performed  
 528 on the wall for its global thermal characterisation in a guarded hot box and for the

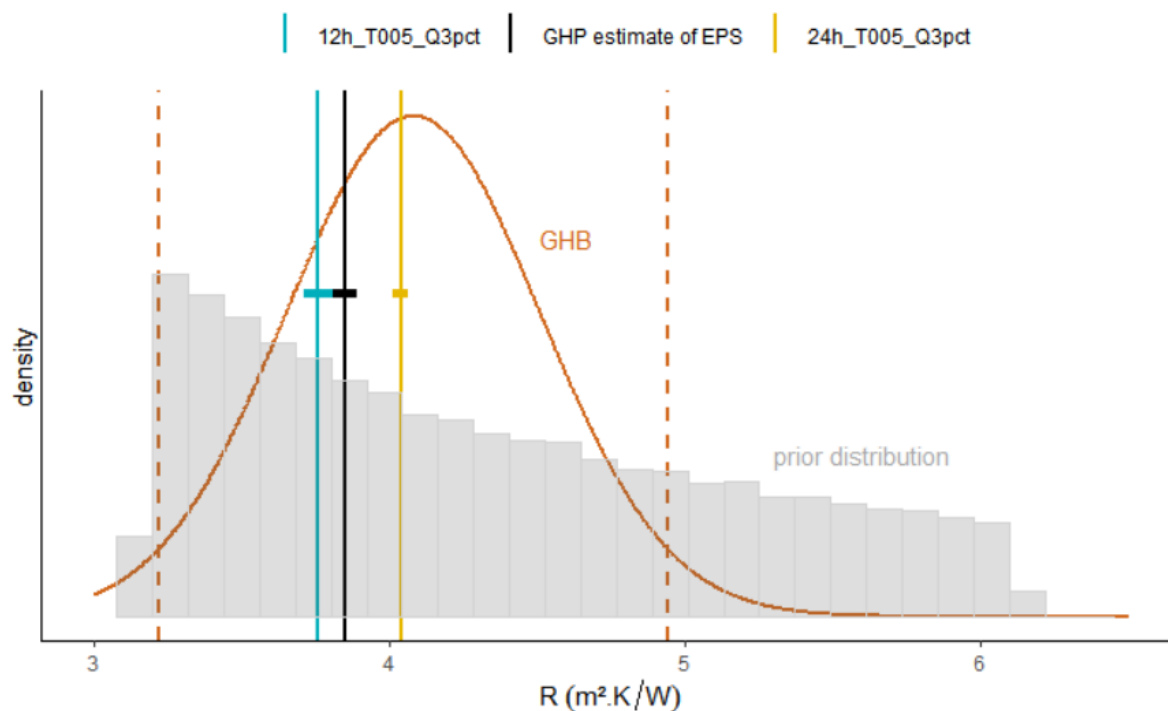


**Figure 10.** In grey: prior distribution of  $R$ , in chocolate: Gaussian distribution associated with the GHB estimate of  $R$  and its 95% coverage interval, in black: GHP estimate of  $R_2$  and its 95% coverage interval, in turquoise: Bayesian estimate of  $R$  after 12 h with the medium uncertainty level and its 95% credible interval, in yellow: Bayesian estimate of  $R$  after 24 h with the medium uncertainty level and its 95% credible interval.

529 thermal characterisation of the insulation layer performed with a guarded hot plate, for  
 530 assessing the performance of the Bayesian uncertainty analysis.

531 The fully Bayesian approach is particularly suited for uncertainty quantification,  
 532 especially when prior knowledge is available, and is used here for its ability to propagate  
 533 input uncertainties in an inversion problem, which is in practice an issue rarely addressed  
 534 with no consensus methodology so far up to our knowledge. The advocated uncertainty  
 535 propagation approach is easy to apply since it consists in treating all uncertain inputs  
 536 as calibration parameters and thus requires only a small adaptation of existing MCMC  
 537 algorithms, for a slightly higher computational cost. For instance, in the case study, we  
 538 experienced that the computational cost comes primarily from the duration.

539 Under the experimental conditions of the climatic chamber equipped with calibrated  
 540 thermocouples and fluxmeters, this study demonstrates the efficiency of the Bayesian  
 541 analysis of the measurements obtained with an active method to produce unbiased (w.r.t  
 542 the guarded hot plate method) estimates of the thermal conductivity of the insulation  
 543 layer (EPS) for 24 hours with a low associated standard uncertainty (less than 2%).  
 544 Nevertheless, smaller observation time, e.g. 12h, has lead to a biased identification.

545 In this application, it appears that the impact of uncertainties is quite small and  
 546 cannot be interpreted in terms of resulting bias w.r.t. a reference value. In particular,

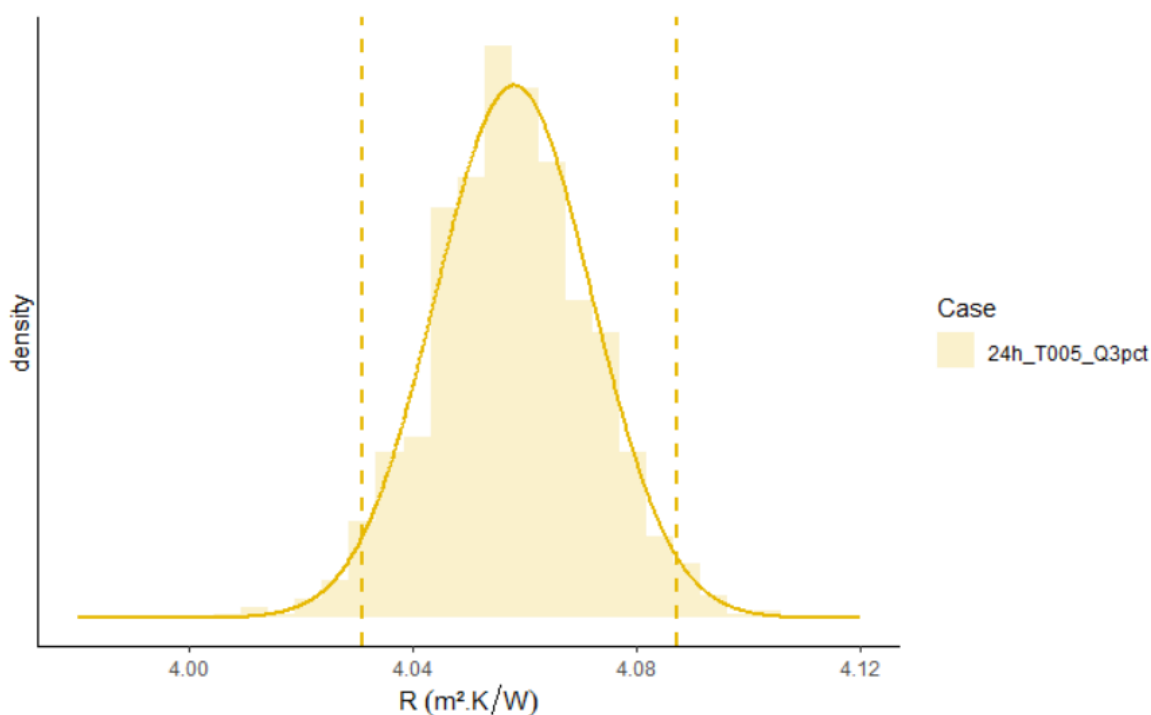


**Figure 11.** Plot of the posterior distribution of the global thermal resistance of the IWI wall obtained with the active method, and its associated 95% credible interval for 24 hours observations (vertical dashed lines).

547 due to the experimental settings we were not able to quantify the impact of input  
548 uncertainties on the estimated thermal parameters.

549 For setting input uncertainties, we recommend to perform calibrations and/or  
550 verifications of measurement means. If no input uncertainties are available, this study  
551 confirms the recommendation from the literature to set a small uncertainty on input  
552 parameters to help reducing bias.

553 The general formulation of the methodology makes it easily applicable to other  
554 types of walls and insulation. In this respect, one of the perspectives of the RESBATI  
555 project is to address sustainable materials like bio-sourced materials and raw earth  
556 considering a hygro-thermal model.

## 557 Acknowledgements

558 This research was made possible by support from ANR (Agence Nationale de la  
559 Recherche) the French National Research Agency through the project RESBATI under  
560 Grant agreement NANR-16-CE22-0010-02.



## References

- [ASHRAE, 2017] ASHRAE (2017). *ASHRAE handbook: Fundamentals : SI edition*. American Society of Heating, Refrigerating and Air-Conditioning Engineers, Atlanta, GA.
- [Berger et al., 2016] Berger, J., Orlande, H. R., Mendes, N., and Guernouti, S. (2016). Bayesian inference for estimating thermal properties of a historic building wall. *Building and Environment*, 106:327 – 339.
- [BIPM et al., 2008a] BIPM, IEC, IFCC, ILAC, ISO, IUPAC, IUPAP, and OIML (2008a). *Guide to the Expression of Uncertainty in Measurement, JCGM 100:2008, GUM 1995 with minor corrections*. BIPM.
- [BIPM et al., 2008b] BIPM, IEC, IFCC, ILAC, ISO, IUPAC, IUPAP, and OIML (2008b). *Supplement 1 to the ‘Guide to the Expression of Uncertainty in Measurement’ – Propagation of distributions using a Monte Carlo method, JCGM 101:2008*. BIPM.
- [Bodnar and Elster, 2014] Bodnar, O. and Elster, C. (2014). On the adjustment of inconsistent data using the birge ratio. *Metrologia*, 51:516.
- [Bodnar et al., 2017] Bodnar, O., Link, A., Arendack, B., Possolo, A., and Elster, C. (2017). Bayesian estimation in random effects meta-analysis using a non-informative prior. *Statistics in Medicine*, 36(2):378–399.
- [Box and Tiao, 1992] Box, G. and Tiao, G. (1992). *Bayesian Inference in Statistical Analysis*. Wiley.
- [Chib and Greenberg, 1995] Chib, S. and Greenberg, E. (1995). Understanding the metropolis-hastings algorithm. *The American Statistician*, 49(4):327–335.
- [Demeyer et al., 2021] Demeyer, S., Fischer, N., and Elster, C. (2021). Guidance on Bayesian uncertainty evaluation for a class of GUM measurement models. *Metrologia*, 58:1–13.
- [François et al., 2020] François, A., Ibos, L., Feuillet, V., and Meulemans, J. (2020). Estimation of the thermal resistance of a building wall with inverse techniques based on rapid active in situ measurements and white-box or ARX blackbox models. *Energy & Buildings*, 226.
- [Gelman et al., 2013] Gelman, A., Carlin, J. B., Stern, H. S., Dunson, D. B., Vehtari, A., and Rubin, D. B. (2013). *Bayesian Data Analysis, 3rd edition*. Chapman and Hall/CRC.
- [Goffart et al., 2017] Goffart, J., Mara, T., and Wurtz, E. (2017). Generation of stochastic weather data for uncertainty and sensitivity analysis of a low-energy building. *Journal of Building Physics*, 41(1):41–57.
- [Gori and Elwell, 2018] Gori, V. and Elwell, C. A. (2018). Estimation of thermophysical properties from in-situ measurements in all seasons: Quantifying and reducing errors using dynamic grey-box methods. *Energy & Buildings*, 167:290 – 300.
- [Ha et al., 2020] Ha, T.-T., Feuillet, V., Waeytens, J., Zibouche, K., Thebault, S., Bouchie, R., Le Sant, V., and Ibos, L. (2020). Benchmark of identification methods for the estimation of building wall thermal resistance using active method: Numerical study for iwi and single-wall structures. *Energy and Buildings*, 224:110130.
- [Heo et al., 2012] Heo, Y., Choudhary, R., and Augenbroe, G. (2012). Calibration of building energy models for retrofit analysis under uncertainty. *Energy and Buildings*, 47:550 – 560.
- [Higdon et al., 2004] Higdon, D., Kennedy, M., Cavendish, J., Cafeo, J., and Ryne, R. (2004). Combining field data and computer simulations for calibration and prediction. *SIAM Journal on Scientific Computing*, 26(2):448–466.
- [Iglesias et al., 2018] Iglesias, M., Sawlan, Z., Scavino, M., Tempone, R., and Wood, C. (2018). Bayesian inferences of the thermal properties of a wall using temperature and heat flux measurements. *International Journal of Heat and Mass Transfer*, 116:417 – 431.
- [ISO 8302:1991, 1991] ISO 8302:1991 (1991). *Thermal Insulation Determination of Steady-State Thermal Resistance and Related Properties Guarded hot plate apparatus*. International Organization for Standardization.
- [ISO 8990:1994, 1994] ISO 8990:1994 (1994). *Thermal insulation - Determination of steady-state thermal transmission properties - Calibrated and guarded hot box*. International Organization

for Standardization.

- [Kaipio and Fox, 2011] Kaipio, J. P. and Fox, C. (2011). The bayesian framework for inverse problems in heat transfer. *Heat Transfer Engineering*, 32(9):718–753.
- [Kennedy and O’Hagan, 2001] Kennedy, M. and O’Hagan, A. (2001). Bayesian calibration of computer models. *J. R. Statist. Soc. B*, 63(3):425–464.
- [Klaunberg and Elster, 2016] Klaunberg, K. and Elster, C. (2016). Markov chain Monte Carlo methods: an introductory example. *Metrologia*, 53(1):S32.
- [Koenen et al., 2019] Koenen, A., Marquis, D., Garcia, Y., Le Sant, V., Demeyer, S., Monchau, J.-P., Feuillet, V., Ibos, L., Ha, T., Gavérina, L., Dumoulin, J., Manceau, J.-L., Bouchié, R., Zibouche, K., and Lahlou, F. (2019). Evaluation of a research prototype for measuring and controlling the thermal resistance of building walls in active mode. *ITCC-ITES Conference*.
- [Macdonald, 2002] Macdonald, I. A. (2002). *Quantifying the effects of uncertainty in building simulation*. University of Strathclyde. PhD thesis.
- [Mana et al., 2012] Mana, G., Massa, E., and Predescu, M. (2012). Model selection in the average of inconsistent data: an analysis of the measured Planck-constant values. *Metrologia*, 49:492500.
- [Metropolis et al., 1953] Metropolis, N., Rosenbluth, A. W., Rosenbluth, M. N., Teller, A. H., and Teller, E. (1953). Equation of state calculations by fast computing machines. *The Journal of Chemical Physics*, 21(6):1087–1092.
- [NF EN ISO 10211:2017, 2017] NF EN ISO 10211:2017 (2017). *Thermal bridges in building construction Heat flows and surface temperatures Detailed calculations*. International Organization for Standardization.
- [NF EN ISO 12567-1:2013, 2013] NF EN ISO 12567-1:2013 (2013). *Thermal performance of windows and doors Determination of thermal transmittance by the hot-box method Part 1: Complete windows and doors*. International Organization for Standardization.
- [Perrin and Durantin, 2019] Perrin, G. and Durantin, C. (2019). Taking into account input uncertainties in the bayesian calibration of time-consuming simulators. *Journal de la Société Française de Statistique*, 160:24 – 46.
- [Rasmussen and Williams, 2006] Rasmussen, C. E. and Williams, C. K. I. (2006). *Gaussian Processes for Machine Learning*. MIT Press.
- [Robert and Casella, 2013] Robert, C. and Casella, G. (2013). *Monte Carlo statistical methods*. Springer Science & Business Media.
- [Rodler et al., 2019] Rodler, A., Guernouti, S., and Musy, M. (2019). Bayesian inference method for in situ thermal conductivity and heat capacity identification: Comparison to iso standard. *Construction and Building Materials*, 196:574 – 593.
- [Rouchier, 2018] Rouchier, S. (2018). Solving inverse problems in building physics: An overview of guidelines for a careful and optimal use of data. *Energy & Buildings*, 166:178 – 195.
- [Saltelli et al., 2004] Saltelli, A., Tarantola, S., Campolongo, F., and Ratto, M. (2004). *Sensitivity Analysis in Practice: A Guide to Assessing Scientific Models*. Wiley.
- [Santner and Notz, 2003] Santner, T. J. and Notz, W. (2003). *The design and analysis of computer experiments*. Springer Verlag, Springer Series in Statistics.
- [Simon et al., 2018] Simon, L. D., Iglesias, M., Jones, B., and Wood, C. (2018). Quantifying uncertainty in thermophysical properties of walls by means of bayesian inversion. *Energy and Buildings*, 177:220 – 245.
- [Thébault and Bouchié, 2018] Thébault, S. and Bouchié, R. (2018). Refinement of the isabele method regarding uncertainty quantification and thermal dynamics modelling. *Energy and Buildings*, 178:182 – 205.
- [Toman and Possolo, 2009] Toman, B. and Possolo, A. (2009). Laboratory effects models for interlaboratory comparisons. *Accreditation and Quality Assurance*, 14:553–563.
- [Wang and Zabaras, 2004] Wang, J. and Zabaras, N. (2004). Hierarchical bayesian models for inverse problems in heat conduction. *Inverse Problems*, 21(1):183–206.
- [XP ISO/TS 28037:2013, 2013] XP ISO/TS 28037:2013 (2013). *Détermination et utilisation des*

662 *fonctions d'étalonnage linéaire.* International Organization for Standardization.

663 **Appendix A. Details on GHB uncertainty evaluation at CSTB, France**

The estimated  $U$  value for the IWI wall for a mean temperature  $T = 10^\circ\text{C}$  is

$$U = 0.245 \text{ W m}^{-2} \text{ K} \quad (\text{A.1})$$

The global thermal resistance is

$$R = \frac{1}{U} \quad (\text{A.2})$$

Denoting  $u(U)$  the standard uncertainty associated with  $U$ , GUM [BIPM et al., 2008a] uncertainty propagation gives

$$u(R) = \frac{u(U)}{U^2} = 0.43 \text{ m}^2 \text{ K W}^{-1} \quad (\text{A.3})$$

Equivalently, the 95% coverage interval associated with  $R$  is

$$4.08 \pm 0.86 \text{ m}^2 \text{ K W}^{-1} (k = 2) \quad (\text{A.4})$$

664 The following describes the uncertainty evaluation of  $U$ . The specimen is installed  
 665 on a surrounding wall, the measurement zone is larger than the sample surface so that,  
 666 in steady state conditions, a part of the heating power injected in the measurement zone  
 667  $\phi_{in}$  is split between :

- 668 • A thermal flow through the metering box,  $\phi_{out}$ , controlled to be neglectable by  
 669 controlling the guarded zone temperature equal to the measuring zone temperature.  
 The residual thermal flow through the metering box is then controlled to be  
 670 neglectable by measuring it using a thermopile ( $\phi_{out} = 0 \text{ W}$ );
- 671 • A thermal flow through the specimen  $\phi_{sp}$ ;
- 672 • A thermal flow through the surrounding wall  $\phi_{sur}$ ;
- 673 • A thermal flow through thermal bridge between the sample and surrounding wall  
 674  $\phi_{edge}$ ;
- 675

The thermal flow through the specimen is then obtained by

$$\phi_{sp} = \phi_{in} - \phi_{sur} - \phi_{edge} \quad (\text{A.5})$$

676 The  $U$  value is then obtained by

$$U = \frac{\phi_{sp}}{A_{sp} (\theta_{n,i} - \theta_{n,e})} \quad (\text{A.6})$$

where  $A_{sp}$  is the surface of the specimen,  $\theta_{n,i}$  and  $\theta_{n,e}$  are the environment internal/external temperatures included by air temperature ( $\theta_{c,i}, \theta_{c,e}$ ) and radiant temperature viewed by the specimen ( $\theta_{r,i}, \theta_{r,e}$ ) temperatures:

$$\theta_{n,i} = F_{c,i}\theta_{c,i} + (1 - F_{c,i})\theta_{r,i} \quad (\text{A.7})$$

$$\theta_{n,e} = F_{c,e}\theta_{c,e} + (1 - F_{c,e})\theta_{r,e} \quad (\text{A.8})$$

677 where  $F_{c,i}$  and  $F_{c,e}$  are convective fractions.

678 Radiant temperatures ( $\theta_{r,i}, \theta_{r,e}$ ) are described in Annex A of NF EN ISO 12567-1  
679 [NF EN ISO 12567-1:2013, 2013] as an explicit function of surface temperatures of the  
680 specimen ( $\theta_{s,i}, \theta_{s,e}$ ) and the baffle ( $\theta_{b,i}, \theta_{b,e}$ ) panel situated in front of each side.

681 The thermal flow through the surrounding wall  $\phi_{sur}$  and convective fractions  $F_{c,i}$   
682 and  $F_{c,e}$  are obtained using a calibration process as described in NF EN ISO 12567-  
683 1 [NF EN ISO 12567-1:2013, 2013]. This calibration consists in using homogeneous  
684 insulated calibration panels as specimen. The thermal resistance of these calibration  
685 panels have been measured using guarded hot plate method so that their R-values are  
686 well known. Measuring surface temperatures during the calibration test in the guarded  
687 hot box make possible determining both  $R_{sur}$  (and then  $\phi_{sur}$ ) as a function of average  
688 support wall temperature, and convective fractions as a function of thermal flow through  
689 the specimen, using linear regression techniques. The linear regression coefficients are  
690 then used to predict  $\phi_{sur}$ ,  $F_{c,i}$  and  $F_{c,e}$  during all experiment. The uncertainty on this  
691 prediction is estimated using less squares methods [XP ISO/TS 28037:2013, 2013].

The uncertainty on the thermal flow through thermal bridge between the  
sample and surrounding wall  $\phi_{edge}$  is estimated by simulating each junction  
[NF EN ISO 10211:2017, 2017]. A sensibility analysis has been provided on each  
unknown input: thermal conductivity of wood element for instance may vary between  
0.13 to 0.18 W/(m.K). The possible variation interval of the calculated psi-values,  
estimated with this sensibility analysis, is then used to define a uniform law with  
standard deviation:

$$u_{\psi_{edge}} = \frac{\psi_{edge_{max}} - \psi_{edge_{min}}}{\sqrt{3}} \quad (\text{A.9})$$

692 Finally, all errors are propagated using GUM recommendations [BIPM et al., 2008a].

## 693 Appendix B. R code

694 The R code associated with the low and medium uncertainty levels implementing 1 is  
695 given in the Supplementary material.

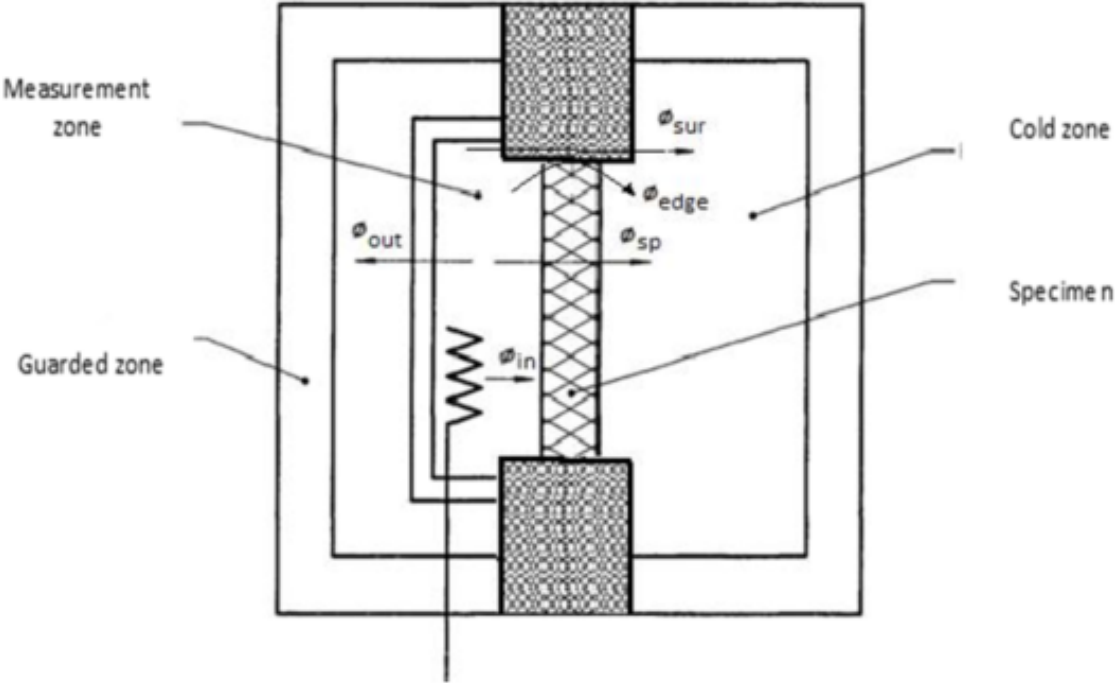


Figure A1. Notations for uncertainty propagation in GHB at CSTB, France.